

Two-particle dispersion in turbulentlike flows

J. C. H. Fung* and J. C. Vassilicos†

*Department of Applied Mathematics and Theoretical Physics, University of Cambridge, Silver Street,
Cambridge CB3 9EW, United Kingdom*

(Received 24 February 1997; revised manuscript received 29 July 1997)

Kinematic simulations are non-Markovian Lagrangian models of dispersion that incorporate turbulentlike flow structure. We investigate the conditions for two-particle dispersion to be local in a turbulentlike flow, and the dependence of the Richardson constant G_Δ on the topology of individual realizations of the flow. [S1063-651X(98)07502-3]

PACS number(s): 47.27.Eq, 47.27.Qb, 47.27.Gs

I. INTRODUCTION

Lagrangian calculations of average concentrations require knowledge of one-particle statistics. However, if Lagrangian calculations of concentration fluctuations and concentration covariances are to account for turbulent mixing associated with relative dispersion, then such calculations must incorporate some features and properties of two-particle statistics [1]. The calculation of concentration covariances is important in the prediction of reaction rates in chemical reactors and in the atmosphere because chemical reaction rates depend on concentration covariances and not on average concentrations. The calculation of concentration fluctuations is also important for air-quality control, combustion, and pollutant dispersal in geophysical flows.

Perhaps the most important statistic of two-particle dispersion (certainly the most frequently studied) is the mean square distance between two fluid elements (also referred to as particles in this paper), $\overline{\Delta^2}(t)$, which is of course a function of time t . In certain circumstances, such as downstream of a linear concentration gradient [1], $\overline{\Delta^2}(t)$ is the only two-particle statistic needed to calculate concentration fluctuations. In general, $\overline{\Delta^2}(t)$ is one of the fundamental quantities of interest in the theory of turbulent dispersion. In a series of papers starting in 1926, Richardson [2] studied the turbulent diffusivity $(d/dt)\overline{\Delta^2}(t)$ as a function of the distance Δ between two particles advected by atmospheric turbulence. Richardson's empirical finding, $(d/dt)\overline{\Delta^2} \sim (\overline{\Delta^2})^{2/3}$, implies $\overline{\Delta^2} \sim t^3$ (neglecting the initial distance Δ_0 between pairs of particles under the assumption that $\Delta_0^2 \ll \overline{\Delta^2}$ at a time t that is sufficiently large). Obukhov [3] and Batchelor [4] derived Richardson's dispersion law theoretically by applying Kolmogorov's similarity arguments to $\overline{\Delta^2}(t)$ and obtained $\overline{\Delta^2}(t) \sim \epsilon t^3$ in an intermediate inertial range of times t (ϵ is the average rate of dissipation per unit mass of fluid). When the time t is much larger than correlation integral time scales, $\overline{\Delta^2}(t) \sim t$ because the two particles move apart independently

[4,5]. When the time t is so small that the particles have only moved in approximate straight lines [4,5], $\overline{\Delta^2}(t) \approx \Delta_0^2 + (\epsilon \Delta_0)^{2/3} t^2$.

One way to formulate the Obukhov-Batchelor similarity theory of relative dispersion is in terms of the "locality assumption," and this assumption is of central concern in this paper. The locality assumption states that, in the inertial range, the dominant contribution to the turbulent diffusivity $(d/dt)\overline{\Delta^2}(t)$ at time t comes from "eddies" of size $(\overline{\Delta^2})^{1/2}(t)$. Hence, $(d/dt)\overline{\Delta^2}(t)$ is a function of $\overline{\Delta^2}$ and ϵ only, and by dimensional arguments, $(d/dt)\overline{\Delta^2}(t) \sim \epsilon^{1/3}(\overline{\Delta^2})^{2/3}$. Provided Δ_0 is below the inertial range of length scales, an integration over time yields

$$\overline{\Delta^2}(t) \approx G_\Delta \epsilon t^3, \quad (1)$$

where G_Δ is a universal dimensionless constant [6].

The value of G_Δ is important for quantitative studies of turbulent dispersion and turbulent concentration fluctuations. The only experimental measurement of G_Δ known to the present authors is that of Tatarski [6]. Unfortunately, Tatarski's measurements and estimations are fraught with uncertainties and there is no point in referring to the actual value that he assigned to G_Δ . Nevertheless we can perhaps say, with some level of confidence, that according to Tatarski's measurements, G_Δ is a number between $O(10^{-2})$ and $O(10^{-1})$ (see the discussion in Fung *et al.* [7]).

To this day, with the one exception of kinematic simulations, no turbulence theory or model gives such a small value of G_Δ . Two-point closures such as LHDIA [8,9] and EDQNM [10] give values between 2.42 and 3.5. Early stochastic models [11,12] lead to $G_\Delta = O(10)$ and more recent stochastic models for two-particle dispersion [13,14] give $G_\Delta = O(1)$. However, kinematic simulations of turbulentlike velocity fields yield G_Δ between $O(10^{-1})$ and $O(10^{-2})$ (Fung *et al.* [7] Sabelfeld [15], Elliott and Majda [16]). Kinematic simulations differ from Lagrangian stochastic models in the qualitative nature of the velocity fields that they generate. Lagrangian stochastic models generate velocities that look like Brownian random walks (with or without drift) in velocity phase space, whereas kinematic simulations generate smoother velocity fields in every realization of the turbulentlike flow. Indeed, kinematic simulations are non-Markovian Lagrangian models of dispersion that incorporate

*Permanent address: Department of Mathematics, The Hong Kong University of Science and Technology, Clear Water Bay, Hong Kong. Electronic address: maifung@uxmail.ust.hk

†FAX: (+44-1223)337918.

Electronic address: jcv10@damtp.cam.ac.uk

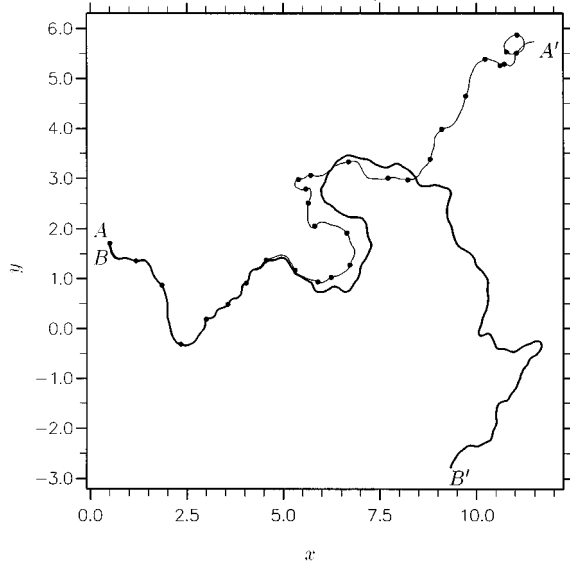


FIG. 1. Kinematic simulation of the flight of two particles (a thick line and a thin line with symbols) in a turbulentlike velocity field with a $k^{-5/3}$ energy spectrum generated as explained in Sec. II A. The particles are initially at points A and B and move closely together until they suddenly separate at two well-identifiable instances, presumably because of hitting a straining region. The trajectories of both particles are also visibly much smoother than Brownian paths and not dissimilar to the turbulent trajectories photographed in Dop *et al.* [17].

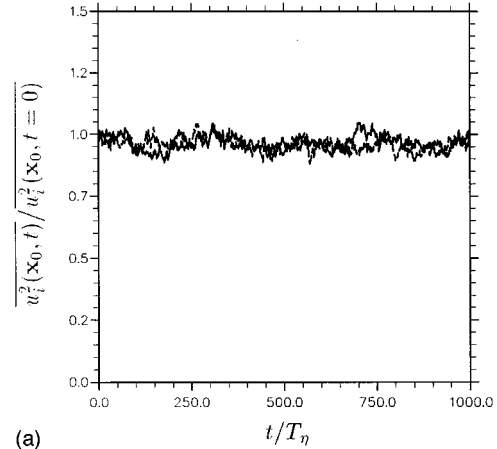
turbulentlike flow structure. It may also be instructive to compare particle trajectories generated by a kinematic simulation (Fig. 1) with the photographs of particle trajectories in turbulent flows reproduced in van Dop *et al.* [17]. Fung *et al.* [7] attempt to explain their low value of G_Δ in terms of the eddying, streaming, and straining regions [see Fig. 10(a)] that appear in individual realizations of their turbulentlike flows. Particle pairs should move together in eddying and streaming regions and only separate abruptly (Fig. 1) when they meet a straining region [see Fig. 10(a)]. Hence, in contrast to Lagrangian stochastic models, the particles are most of the time moving together, which may explain why kinematic simulations generate smaller values of G_Δ than Lagrangian stochastic models. Elliott and Majda [16] are mostly concerned with the prowess of their numerical code and make no attempt to explain their low value of G_Δ . However, they do emphasize that their velocity field is fractal and that, following the suggestion in Sabelfeld [15], the time dependence of their turbulentlike velocity field is introduced by a constant-velocity sweeping of an otherwise frozen velocity field.

In this paper an attempt is made to address the following two questions:

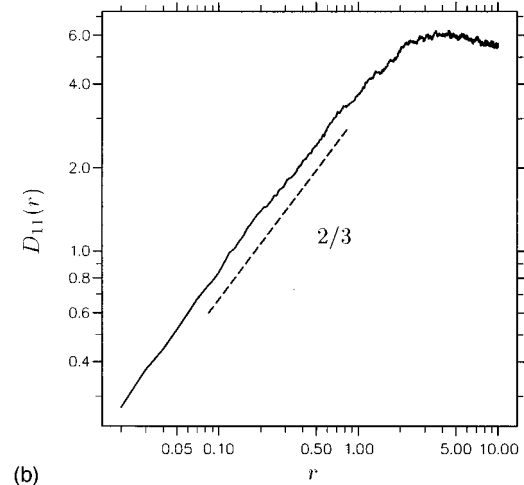
(i) What parameters of the velocity field influence the inertial range power-law behavior of the turbulent relative separation of particles, i.e., $\overline{\Delta^2(t)} \sim t^3$?

(ii) How does G_Δ depend on the parameters and the topology of individual flow realizations?

In the next section we describe the turbulentlike velocity field that we generate to study two-particle dispersion and we discuss the consequences that the locality assumption has on



(a)



(b)

FIG. 2. (a) Plot of $\overline{u_i^2(\mathbf{x}_0, t)/u_i^2(\mathbf{x}_0, t=0)}$ against t/T_η (solid line for $i=1$ and dashed line for $i=2$) demonstrating that the flow field is stationary in time. In this particular plot $p=5/3$, $2\pi/L=1.1$, $2\pi/\eta=1860$, $\Delta_0=\eta/2$, and $\omega_n=\lambda k_n^{(3-p)/2}$ with $\lambda=0.5$, and the wave numbers k_n are geometrically distributed with $N_k=79$. Similar stationary behaviour is observed for an algebraic distribution of wave numbers and for different values of the above parameters. The ensemble average is calculated over 2000 realizations. (b) Log-log plot of the structure function $D_{11}(r)=[u_1(x+r, y, t)-u_1(x, y, t)]^2$ against r for $p=5/3$. The dashed line has a $2/3$ slope for comparison, indicating that $D_{11}(r)$ has a $2/3$ slope over about two decades. The ensemble average is over 2000 realizations. The plot has been obtained for the same parameter values as (a) (similar behavior is observed for an algebraic distribution of wave numbers).

this velocity field's relative dispersion properties. The results of our simulations are presented in Sec. III and we conclude in Sec. IV.

II. THE TURBULENTLIKE VELOCITY FIELD AND THE LOCALITY ASSUMPTION

A. The velocity field

We follow the approach of Turfus and Hunt [18], Sabelfeld [15], and Fung *et al.* [7] and generate on the computer an incompressible two-dimensional (2D) turbulentlike velocity field $\mathbf{u}(\mathbf{x}, t)$ that is identical to that of Vassilicos and Fung [19], i.e.,

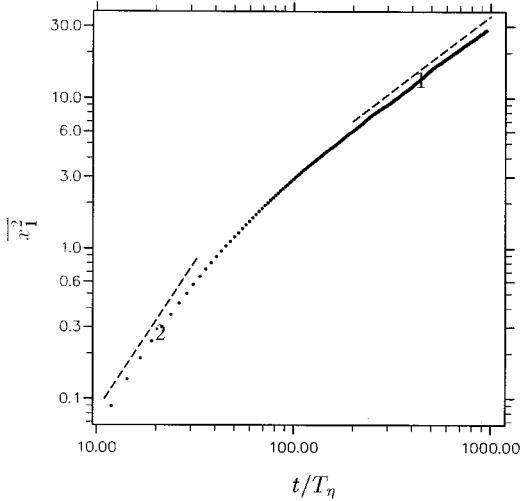


FIG. 3. Log-log plot of the mean square displacement of fluid elements from a fixed point in an isotropic stationary and homogeneous turbulentlike flow (2). The solid dots are the computational result and the dashed lines represent different slopes, i.e., $\overline{x_1^2} \propto t^2$ when $t \ll T_L$ and $\overline{x_1^2} \propto t$ when $t \gg T_L$. The ensemble average is over 2000 realizations. The plot has been obtained for the same parameter values as Fig. 2(a) (similar behavior is observed for an algebraic distribution of wave numbers and different values of λ).

$$\mathbf{u}(\mathbf{x}, t) = \sum_{n=1}^{N_k} [\mathbf{A}_n \cos(\mathbf{k}_n \cdot \mathbf{x} + \omega_n t) + \mathbf{B}_n \sin(\mathbf{k}_n \cdot \mathbf{x} + \omega_n t)], \quad (2)$$

where N_k is the number of modes in the simulations and the Cartesian coordinates of \mathbf{A}_n , \mathbf{B}_n , and \mathbf{k}_n are given by $\mathbf{A}_n = A_n (\cos \phi_n, -\sin \phi_n)$, $\mathbf{B}_n = B_n (-\cos \phi_n, \sin \phi_n)$, and $\mathbf{k}_n = k_n (\sin \phi_n, \cos \phi_n)$. The angles ϕ_n are random and uncorrelated with each other and the velocity field (2) is incompressible because $\mathbf{A}_n \cdot \mathbf{k}_n = \mathbf{B}_n \cdot \mathbf{k}_n = 0$ for all n . The positive amplitudes A_n and B_n are chosen according to

$$A_n^2 = B_n^2 = E(k_n) \Delta k_n, \quad (3)$$

where $E(k)$ is a prescribed Eulerian energy spectrum of the form

$$E(k) = E_0 L (kL)^{-p} \quad (4)$$

in the range $2\pi/L = k_1 \leq k \leq k_{N_k} = 2\pi/\eta$ and such that $E(k) = 0$ outside this range. $\Delta k_n = (k_{n+1} - k_{n-1})/2$ for $2 \leq N_k \leq N_k - 1$, $\Delta k_1 = (k_2 - k_1)/2$ and $\Delta k_{N_k} = (k_{N_k} - k_{N_k-1})/2$. The distribution of wave numbers k_n is either algebraic or geometric, i.e.,

$$k_n = \begin{cases} k_1 n^\alpha & (\text{algebraic}) \\ k_1 a^{n-1} & (\text{geometric}), \end{cases}$$

where α and a are dimensionless numbers that are functions of L/η and N_k because $k_{N_k} = 2\pi/\eta$. [Hence $\alpha = \ln(L/\eta)/\ln N_k$ and $a = (L/\eta)^{1/(N_k-1)}$, respectively.]

The frequencies ω_n in Eq. (2) determine the unsteadiness associated with wave mode n . We experiment with two different models of unsteadiness: (i) a model [7,19] where the

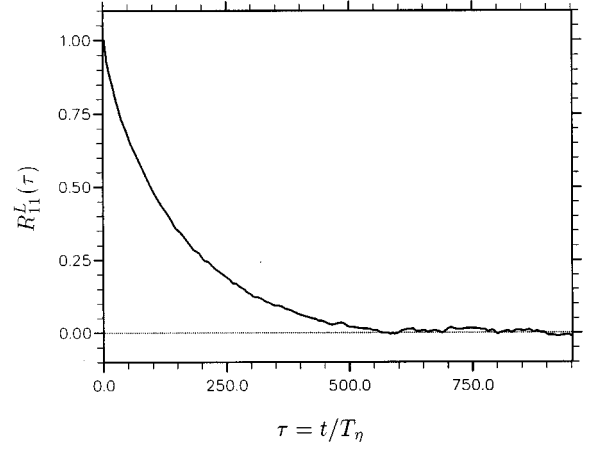


FIG. 4. The Lagrangian autocorrelation function $R_{11}^L(\tau)$ against $\tau = t/T_\eta$. From this graph, T_L is obtained to be $T_L \approx 143T_\eta$ in good agreement with Fig. 3. This plot has been obtained for the same parameter values as Fig. 3.

unsteadiness frequency ω_n is proportional to the eddy turnover time of wave mode n , i.e.,

$$\omega_n = \lambda \sqrt{k_n^3 E(k_n)}, \quad (5)$$

where λ is a dimensionless constant, and (ii) a model [16,18] where all the wave modes are advected with a constant velocity U , i.e.,

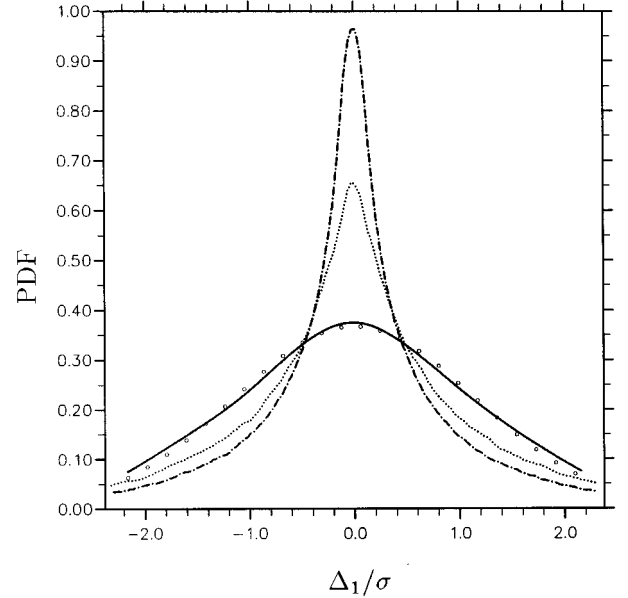


FIG. 5. PDF of the separation vector component Δ_1/σ at different times, $t = 858T_\eta$ (dot-dashed line), $t = 1716T_\eta$ (dotted line), and $t = 4290T_\eta$ (solid line). At the largest time $t = 4290T_\eta$, the data agree very closely with the Gaussian distribution of the same standard deviation (circles) but cannot be fitted by a Gaussian at the earlier times of this plot. This plot has been obtained for $N_k = 100$, $p = 5/3$ and a geometric distribution of wave numbers (similar results are obtained with an algebraic distribution). The unsteadiness parameter $\lambda = 0.5$ and the other parameters of the turbulentlike flow are $p = 5/3$, $2\pi/L = 1.1$, $2\pi/\eta = 1860$, and $\Delta_0 = \eta/2$.

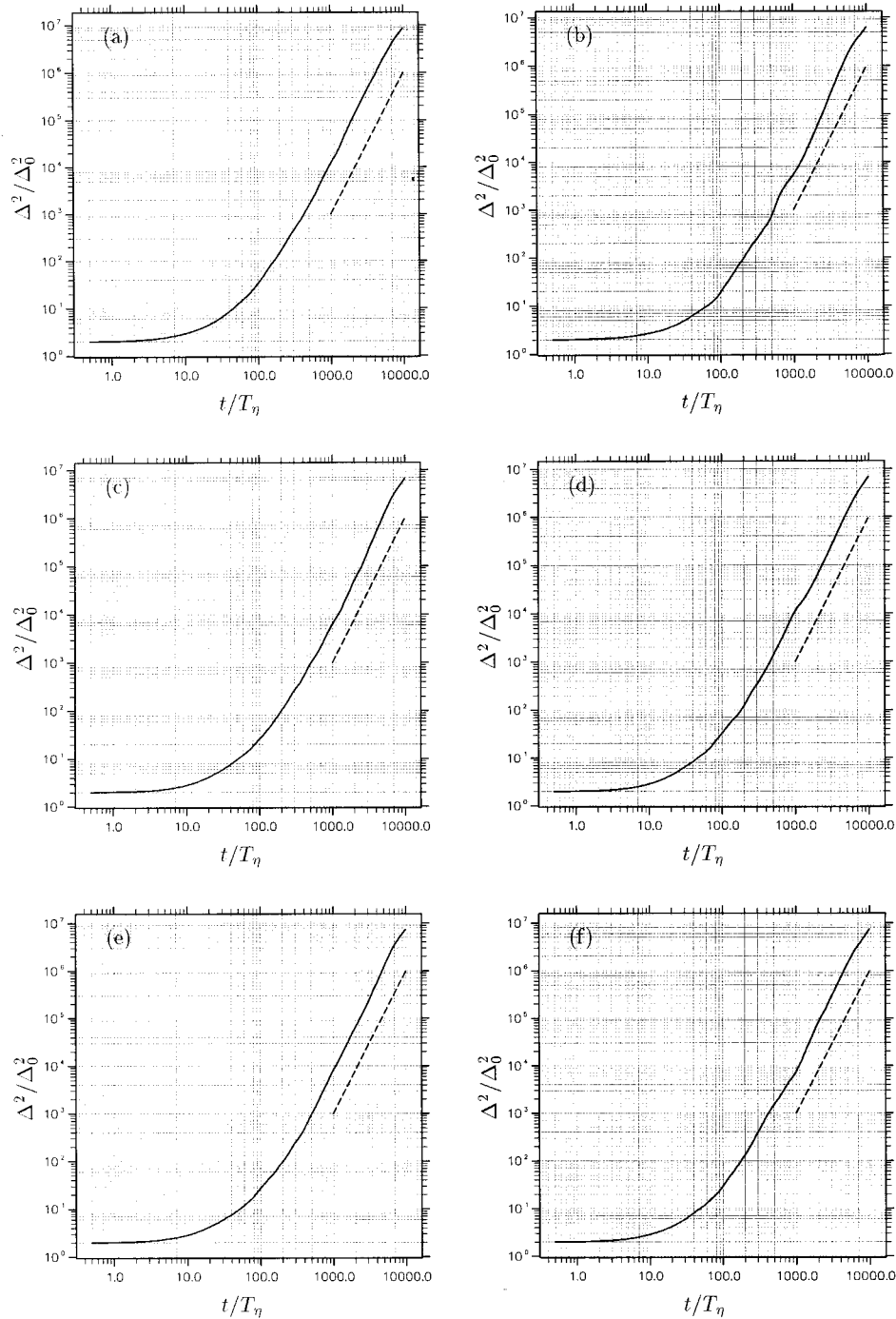


FIG. 6. Log-log plots of $\overline{\Delta^2}/\Delta_0^2$ against t/T_η , where $T_\eta = \eta/\sqrt{E_0}$. These plots have been obtained for $p=5/3$, $2\pi/L=1.1$, $2\pi/\eta = 1860$, $\Delta_0 = \eta/2$, and unsteadiness parameter $\omega_n = \lambda k_n^{(3-p)/2}$ with $\lambda=0.5$. The averages were calculated over 2000 particle pairs and $T_L/T_\eta = 1693$, where $T_L = L/\sqrt{E_0}$. The wave numbers k_n are distributed either algebraically (AD) or geometrically (GD). (a) GD and $N_k = 79$, (b) AD and $N_k = 20$, (c) AD and $N_k = 40$, (d) AD and $N_k = 79$, (e) AD and $N_k = 125$ and (f) AD and $N_k = 158$. The dashed line is a line with slope equals to 3.

$$\omega_n = Uk_n. \quad (6)$$

The turbulentlike velocity fields simulated here are stationary in time [see Fig. 2(a)] and their spatial structure function $D_{11}(r) = [u_1(x+r, y, t) - u_1(x, y, t)]^2 \sim r^{p-1}$ over a significant range of length scales (see Fig. 2(b)).

This kinematically simulated velocity field is 2D in the sense that it has two components. There are of course no dynamics, whether 2D or 3D, in such simulations. Instead, we prescribe the power p that characterizes the energy spectrum's scaling, and in this paper values of p are chosen between $p=1$ and $p=3$. The advantage of studying a 2D rather than a 3D flow is that flow topology is significantly simpler

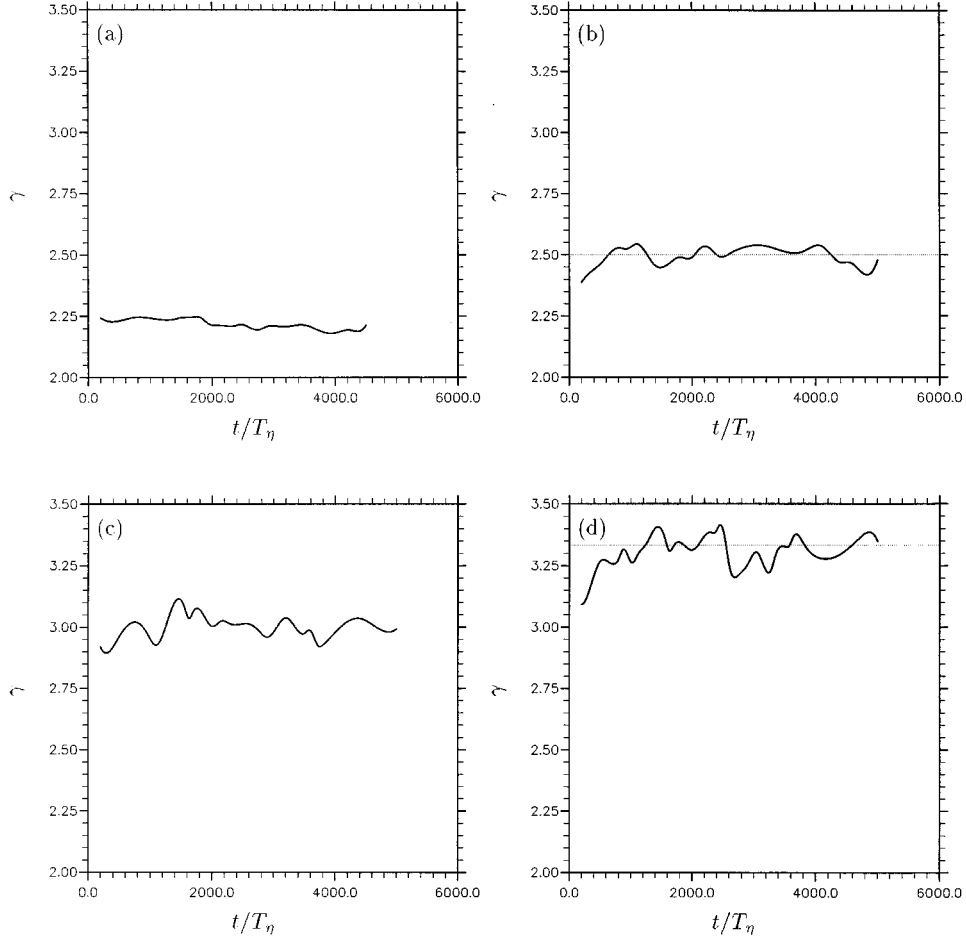


FIG. 7. Linear plots of the power γ defined in Eq. (9) against t/T_η , where $T_\eta = \eta/\sqrt{E_0}$. These plots have been obtained for the same parameter values as Fig. 6 and a geometric distribution of wave numbers with $N_k = 79$ (except for (a) and (b) where the highest wave number is $2\pi/\eta = 4000$ and $N_k = 87$). (Similar results are obtained with an algebraic distribution of wave numbers.) (a) $p = 1.2$, (b) $p = 1.4$, (c) $p = 1.6667$, and (d) $p = 1.8$, respectively. The dashed line has a value equal to $4/(3-p)$ for comparison. The values of γ oscillate slightly around $4/(3-p)$ thus confirming the validity of Eq. (10). The values of γ are calculated by taking the logarithmic derivative of $\overline{\Delta^2}$ versus t .

in 2D. However, the results obtained in this paper's study of 2D turbulentlike flows should not be extrapolated to 3D turbulentlike flows without further analysis, which is beyond this paper's scope.

B. The locality assumption

The mean square distance $\overline{\Delta^2}(t)$ between two fluid elements that are advected by the turbulentlike velocity field (2) is a function of the following parameters:

$$\overline{\Delta^2} = \overline{\Delta^2}(t, L, \eta, \Delta_0, E_0; p, N_k, \lambda) \quad (7a)$$

if the unsteadiness is simulated as in Eq. (5) and

$$\overline{\Delta^2} = \overline{\Delta^2}(t, L, \eta, \Delta_0, E_0, U; p, N_k) \quad (7b)$$

if the unsteadiness is simulated as in Eq. (6). The first set of parameters in Eq. (7) is a set of dimensional parameters, while the second is a set of dimensionless parameters. In either case, dimensional analysis is inconclusive unless a strong additional assumption is introduced. In the present

context the locality assumption states that in the limit where the Reynolds number $\text{Re} \sim (L/\eta)^{4/3}$ tends to infinity and in an intermediate range of times, $\max(\eta, \Delta_0)/\sqrt{E_0} \ll t \ll L/\sqrt{E_0}$, the only dimensional parameters affecting $\overline{\Delta^2}$ are t and the energy density at $k = \sqrt{1/\Delta^2}$, i.e., $E(\sqrt{1/\Delta^2}) = E_0 L (L^2/\Delta^2)^{-p/2}$. Hence, in these limits, Eq. (7a) may be replaced by

$$\overline{\Delta^2} = \overline{\Delta^2}(t, E(\sqrt{1/\Delta^2}); p, N_k, \text{Re}, \lambda) \quad (8a)$$

and Eq. (7b) by

$$\overline{\Delta^2} = \overline{\Delta^2}\left(t, E(\sqrt{1/\Delta^2}); p, N_k, \text{Re}, \frac{U}{\sqrt{E_0}}\right). \quad (8b)$$

At this stage dimensional requirements yield [20]

$$\overline{\Delta^2} = G_\Delta (E_0 L^{1-p})^{2/(3-p)} t^\gamma, \quad (9)$$

where

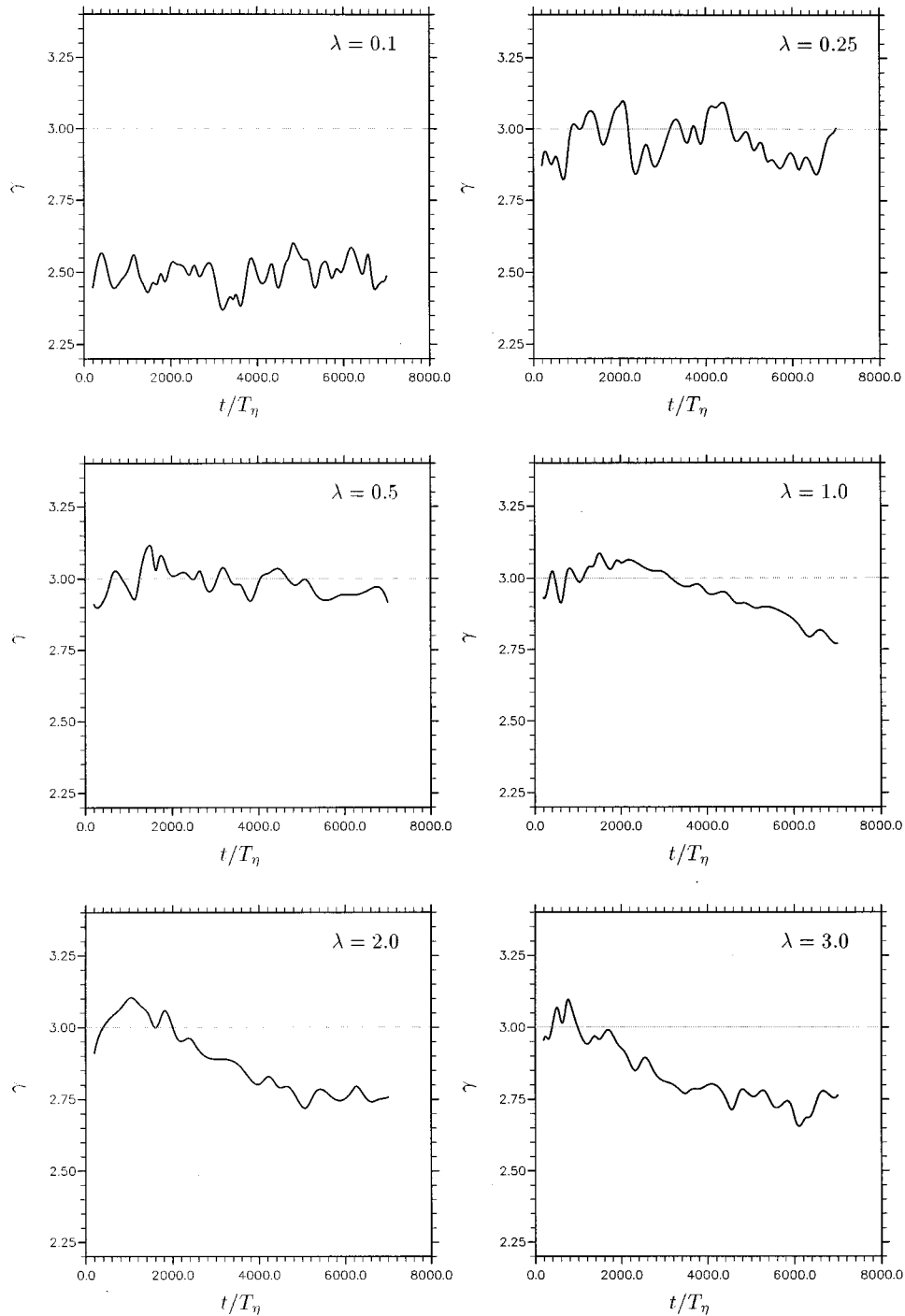


FIG. 8. Linear plots of the power γ defined in Eq. (9) against t/T_η , where $T_\eta = \eta/\sqrt{E_0}$. These plots have been obtained for $N_k=79$, $p=5/3$ and a geometric distribution of wave numbers (similar results are obtained with an algebraic distribution). The unsteadiness parameter λ is varied from 0.1 to 3.0 and the other parameters of the turbulentlike flow are the same as in Fig. 6, i.e., $2\pi/L=1.1$, $2\pi/\eta=1860$, and $\Delta_0=\eta/2$.

$$\gamma = \frac{4}{3-p} \tag{10}$$

It is only for $p < 3$ that Eqs. (9) and (10) can be deduced from Eq. (8) and more generally from the locality assumption. [The locality assumption can also be formulated for $(d/dt)\Delta^2$ but in two different ways: either $(d/dt)\Delta^2 = f(\Delta^2, E(\sqrt{1/\Delta^2}))$ or $d/dt\Delta^2 = f(t, E(\sqrt{1/\Delta^2}))$, where the

dependence on dimensionless parameters is implicit in function f . Both formulations lead to Eqs. (9) and (10) by dimensional arguments provided that $p < 3$. However, when $p = 3$ the first formulation leads to $\ln(\Delta^2/\Delta_0^2) \sim \sqrt{E_0}t/L$, while the second leads to $\ln(\Delta^2/\Delta_0^2) \sim (\sqrt{E_0}t/L)^{4/3}$. The consequences of the locality assumption when $p > 3$ are absurd.] Note that Eqs. (9) and (10) are equivalent to Eq. (1) when $p = 5/3$ because $\gamma = 3$ and $(E_0L^{1-p})^{2/(3-p)} = (\sqrt{E_0})^3/L$, which is pro-

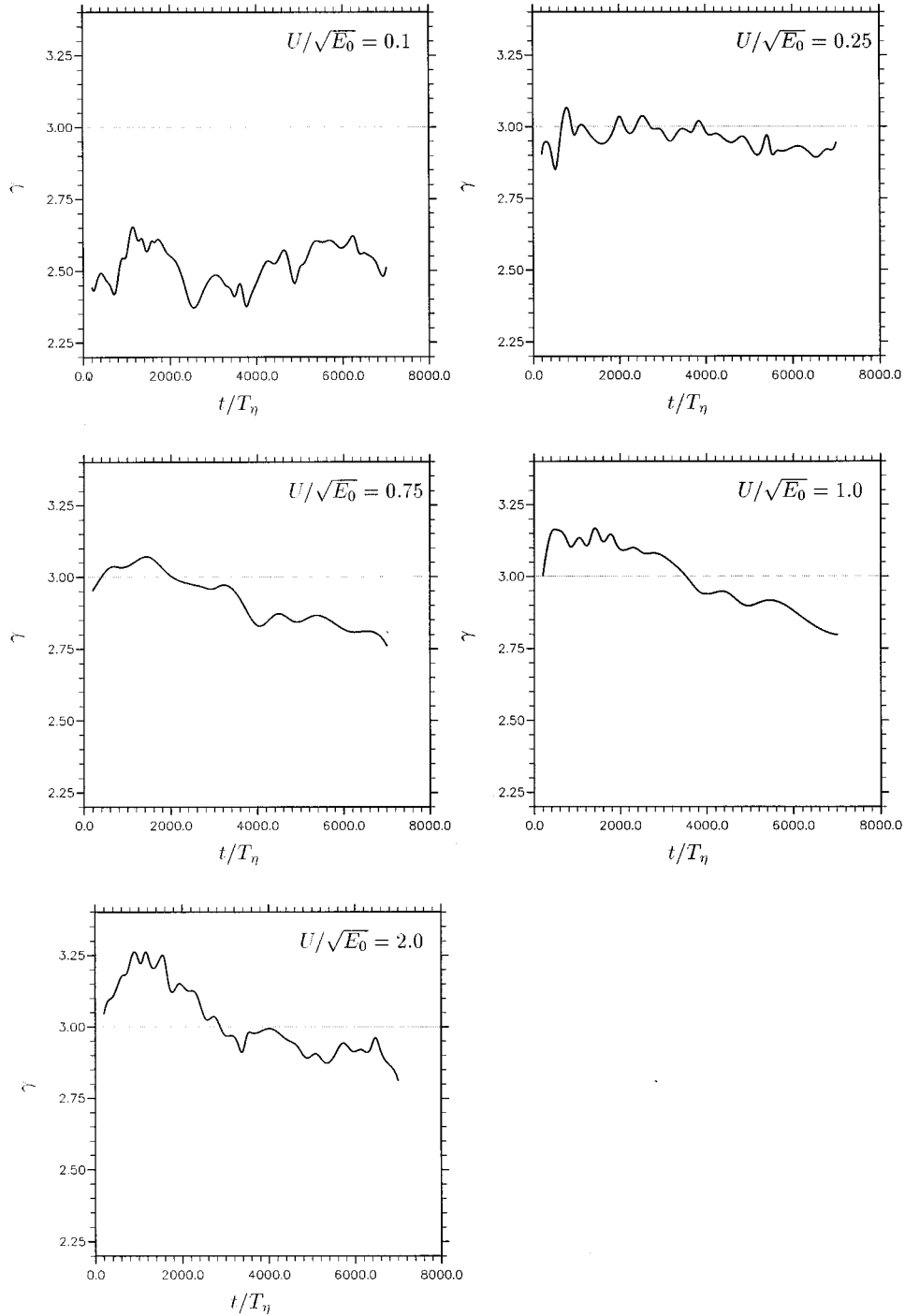


FIG. 9. Linear plots of the power γ defined in Eq. (9) against t/T_η , where $T_\eta = \eta/\sqrt{E_0}$. These plots have been obtained for $N_k=79$, $p=5/3$ and a geometric distribution of wave numbers (similar results are obtained with an algebraic distribution). The unsteadiness parameter $U/\sqrt{E_0}$ is varied from 0.1 to 2.0 and the other parameters of the turbulentlike flow are the same as in Fig. 6, i.e., $2\pi/L=1.1$, $2\pi/\eta=1860$, and $\Delta_0=\eta/2$.

portional to ϵ in high Reynolds number equilibrium turbulence [21]. In this derivation, the constant G_Δ is a function of the dimensionless numbers p , N_k and either λ or $U/\sqrt{E_0}$.

In the following section we investigate the conditions under which Eqs. (9) and (10) are valid, and by induction the conditions under which the locality of two-particle dispersion is valid in a turbulentlike velocity field. These are conditions on the topology and temporal structure of individual realizations of the flow. We also investigate the dependence

of G_Δ on dimensionless parameters of the flow by which token we attempt to reach some insight into the dependence of G_Δ on the topology and temporal structure of the flow.

III. RESULTS

Particle trajectories $\mathbf{x}(t)$ are obtained by integrating

$$\frac{d}{dt} \mathbf{x}(t) = \mathbf{u}(\mathbf{x}(t), t) \quad (11)$$

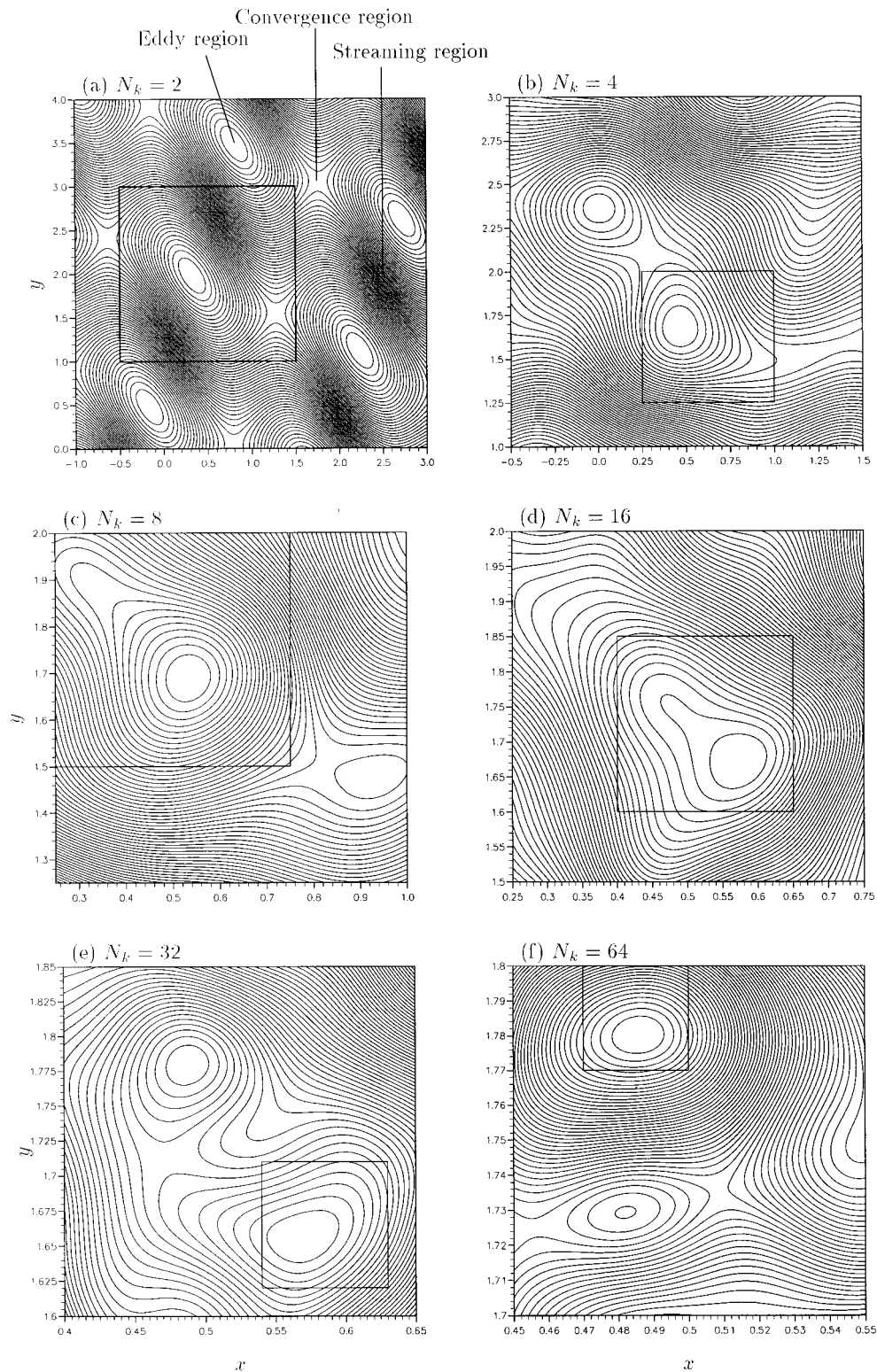


FIG. 10. Instantaneous streamline pattern of the turbulentlike velocity field (2) with $p=5/3$ as one zooms into smaller scales of the velocity field. This is achieved by simultaneously increasing N_k and focusing into inserted smaller regions of the field. (a) $N_k=2$, where we also point at eddying, straining, and streaming regions. (b) Magnified picture of the square region marked inside (a) with $N_k=4$. (c) Magnified picture of the square region marked inside (b) with $N_k=8$. (d) Magnified picture of the square region marked inside (c) with $N_k=16$. (e) Magnified picture of the square region marked inside (d) with $N_k=32$. (f) Magnified picture of the square region marked inside (e) with $N_k=64$. (g) Magnified picture of the square region marked inside (f) with $N_k=128$. (h) Magnified picture of the square region marked inside (g) with $N_k=256$. In all these plots $2\pi/L=2$ and the distribution of wave numbers is geometric, $k_n=(2\pi/L)2^{n-1}$. A similar fractal-eddy structure is also observed for algebraic distributions of wave numbers, but one needs to go up to a much higher number of zoom-in iterations and values of N_k to repeatedly see the eddying region breaking up into two or more smaller and inserted eddying regions.

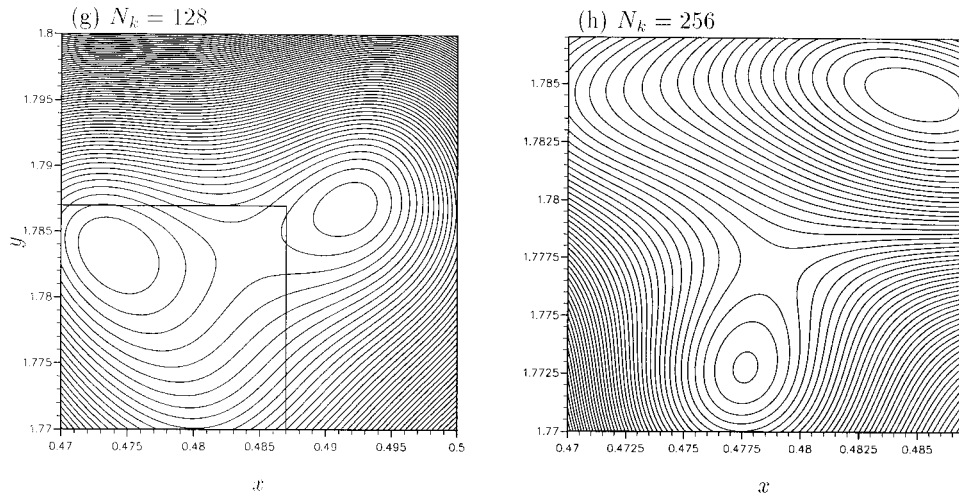


FIG. 10 (Continued).

numerically with an adaptive step-size control scheme for fourth-order Runge-Kutta [22] where the time step is always smaller than all the time scales of the velocity field (see Ref. [19] for details.) When $\mathbf{u}(\mathbf{x}, t)$ is given by a turbulentlike velocity field such as Eq. (2) the particle trajectories are generated by a Lagrangian model of turbulent dispersion called kinematic simulation (KS), which incorporates turbulentlike flow structures, namely, eddying, straining, and streaming regions.

A. One-particle dispersion

We start with a simple demonstration of the dispersive power of the turbulentlike velocity field Eq. (2). Figure 3 is a log-log plot of the one-particle mean square displacement of the first component (same for the second component because of isotropy) $\overline{x_1^2}$ as a function of time. This figure illustrates the result (which we verified for a large variety of parameters p , N_k , and λ or U) that $\overline{x^2} \sim t^2$ for small t and $\overline{x^2} \sim t$ for large t , well in agreement with classical predictions by Taylor [23]. We also calculate the Lagrangian autocorrelation function $R_{11}^L(\tau) = \overline{u_1^L(t)u_1^L(t+\tau)}/u'^2$ where $u_1^L(t) = u_1(\mathbf{x}(t), t)$, $\mathbf{x}(t)$ is given by Eq. (11) and u' is the root-mean-square intensity of one-component turbulence fluctuations. An example is given in Fig. 4. From $R_{11}^L(\tau)$ we derive $T_L = \int_0^\infty R_{11}^L(\tau) d\tau$, and verify that $\overline{x^2} \approx u'^2 t^2$ for $t \ll T_L$ and $\overline{x^2} \approx 2u'^2 T_L t$ for $t \gg T_L$ in complete agreement with Taylor's formulas [23].

We now turn to the study of two-particle dispersion in turbulentlike velocity fields (2). The separation vector Δ between two particles has two components, $\Delta = (\Delta_1, \Delta_2)$ and $\Delta^2 = \Delta_1^2 + \Delta_2^2$. In Fig. 5 we plot an example of the PDF of Δ_1/σ for various times, where $\sigma^2(t)$ is the variance of the component separation Δ_1 at time t . This PDF is the same as that of Δ_2/σ because of isotropy and is markedly non-Gaussian except at very late times when it is very well fitted by a Gaussian distribution of variance $4u'^2 T_L t$, as indeed expected because $\overline{\Delta_1^2} \approx 2\overline{x^2} \approx 4u'^2 T_L t$ at these large times. Note that the plotted PDF is normalized to have unit variance, thus better illustrating the non-Gaussian effects at early times. The remainder of this paper is concerned with two-

particle dispersion in the range of times where the PDF of Δ_1 is not Gaussian.

B. Locality scaling

Figure 6 shows examples of log-log plots of $\overline{\Delta^2}$ versus time t where the power law (9) and (10) is observed to be well defined over nearly two decades irrespective of the number of modes N_k or the distribution of the wave numbers k_n (whether algebraic or geometric). More important for the existence of a well-defined locality scaling (9) and (10) seem to be the ratio L/η and the parameter governing the unsteadiness, λ or U . Indeed, we find that the scaling (9) and (10) is not well defined unless the Reynolds number $\text{Re} = (L/\eta)^{4/3}$ is large enough and in Fig. 6 $\text{Re} \approx 20\,145$. Figure 6(c) shows that the locality scaling is well defined at such high a Reynolds number even with as few as $N_k = 40$ modes. However, it is also found that if N_k is excessively low, that is below 20 at the high Reynolds number of Fig. 6(b), the locality scaling (9) and (10) does not hold (note that the slope in Fig. 6(b) is larger than 3). These observations are relevant because it is important to know that the locality scaling (9) and (10) can be observed with as few as 40 modes of randomly chosen directions.

Figure 7 testifies to the validity of Eqs. (9) and (10) for four different values of p . In these figures the Reynolds number is as high as in Fig. 6, with $k_\eta = 4000$, $N_k = 87$ for (a) and (b), and with $k_\eta = 1860$, $N_k = 79$ for (c) and (d). The unsteadiness parameter is carefully chosen to be $\lambda = 0.5$ so that Eqs. (9) and (10) are valid over a significant range.

The existence and extent of a locality scaling depend crucially on the parameter λ or U governing the unsteadiness of the flow. In Figs. 8 and 9 the power γ defined in Eq. (9) is plotted as a function of time t for different values of λ (Fig. 8) and U (Fig. 9); the dotted horizontal line marks the constant value of γ according to Eq. (10). As illustrated by these figures we find that Eqs. (9) and (10) are valid when λ is around 0.25 to 0.5 or $U/\sqrt{E_0}$ near 0.25. For smaller values of λ or $U/\sqrt{E_0}$, the power law $\overline{\Delta^2} \sim t^\gamma$ seems to hold but the power γ is not given by Eq. (10); and for larger values of λ or $U/\sqrt{E_0}$, the power law (9) and (10) does not hold over a significant range of times.

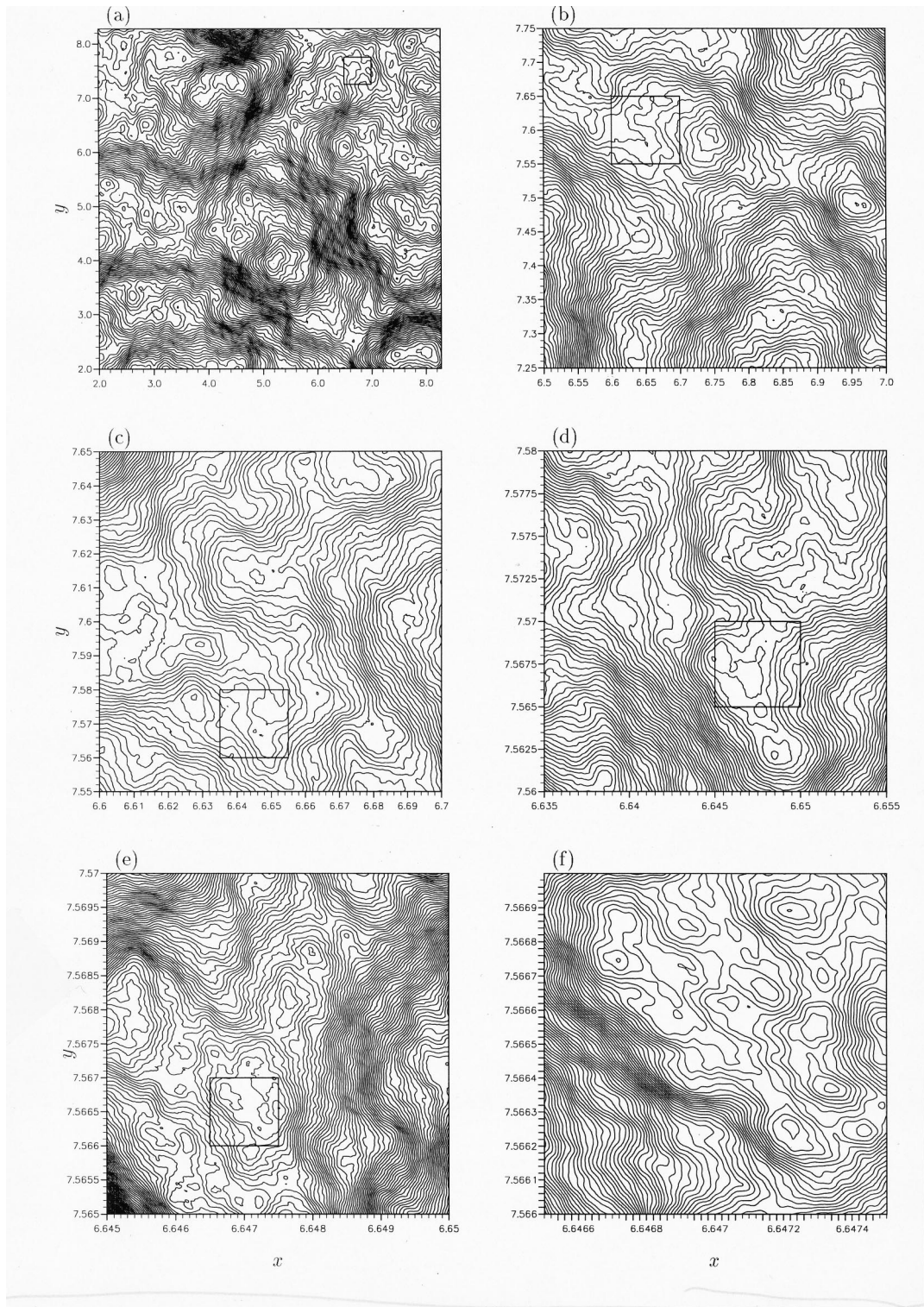


FIG. 11. Instantaneous streamline pattern of the turbulentlike velocity field (2) with $p = 5/3$ as one zooms into smaller scales of the velocity field. In contrast to Fig. 10, here we plot the full L by L field at $N_k = 128$ and then successively magnify smaller regions of the field. (a) A full L by L field. (b) Magnified picture of the square region marked inside (a). (c) Magnified picture of the square region marked inside (b). (d) Magnified picture of the square region marked inside (c). (e) Magnified picture of the square region marked inside (d). (f) Magnified picture of the square region marked inside (e). In all these plots $2\pi/L = 1$ and the distribution of wave numbers is geometric, $k_n = (2\pi/L)1.1^{n-1}$. A similar fractal-eddy structure is also observed for algebraic distributions of wave numbers, but one needs to go up to a much higher number of zoom-in iterations and values of N_k to see eddying region breaking up into smaller eddying regions a sufficient number of times.

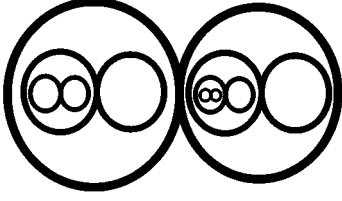


FIG. 12. Schematic interpretation of the fractal-eddy structure revealed in Figs. 10 and 11. The streamline pattern consists of increasingly small cat's eyes. More and smaller cat's eyes are formed in the field as η decreases and $\text{Re}=(L/\eta)^{4/3}$ increases.

The condition $\lambda=0.5$ for the existence of the locality scaling (9) and (10) means that the turbulentlike velocity field should be neither frozen [$\omega_n \ll \sqrt{k_n^3 E(k_n)}$] nor effectively structureless [$\omega_n \gg \sqrt{k_n^3 E(k_n)}$]. The condition $U \sim \sqrt{E_0}$ can perhaps be interpreted in similar terms and in fact Elliott and Majda [16] enforce the same condition to obtain the locality scaling (9) and (10) over eight to twelve decades. [We note, however, that Sabelfeld [15] obtains a scaling (9) and (10) with $U=0$ in a 3D turbulentlike velocity that is therefore frozen. 3D velocity fields are topologically different from 2D velocity fields and the conditions on λ and U for the scaling (9) and (10) to be valid can be significantly different.]

We noted in the previous section that the locality assumption does not imply a power law such as Eq. (9) if $p \geq 3$. There is in fact a dramatic difference in the topology of the flow below and above $p=3$. For $p < 3$ turbulentlike velocity fields such as those considered here have a fractal-eddy structure (see Figs. 10 and 11), which we schematically interpret as consisting of cat's eyes within cat's eyes (Fig. 12). This fractal-eddy structure is most readily revealed by zooming into eddy regions of the flow, but it can also be seen by

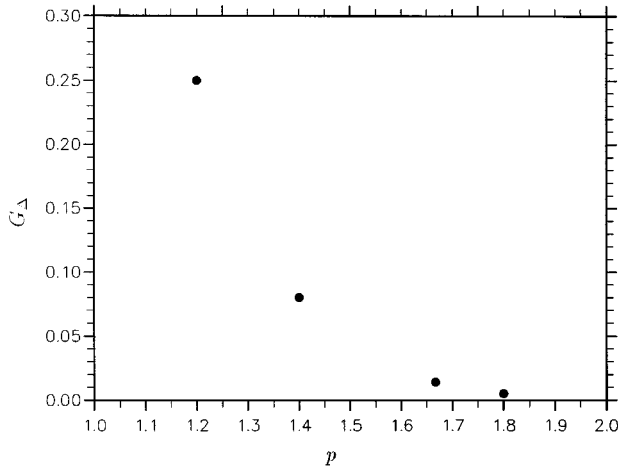


FIG. 13. Linear plot of G_{Δ} against the power p . The parameters of the turbulentlike flow are the same as in Fig. 7. The value of G_{Δ} at time t is obtained by fitting a straight line to the curves similar to Fig. 6 over a small interval around t and G_{Δ} is given by the intersection of this straight line with the x axis. Similar behavior is observed for an algebraic distribution of wave numbers.

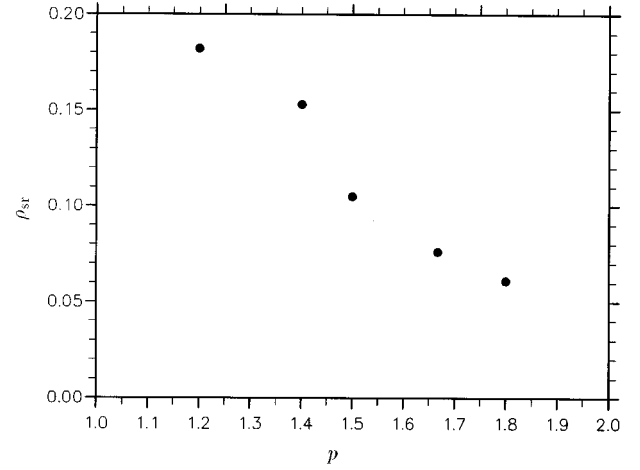


FIG. 14. Linear plot of the straining-region density ρ_{sr} against the power p . The straining-region density is the fraction of the area where $II > II_{rms}$, where II_{rms} is the root-mean-square value of II for the particular value of p . The straining-region density is obtained by averaging II over 50 realizations and over a uniform grid of 200 by 200 (i.e., 40 000 points) in an area of $5L$ by $5L$. This particular plot has been obtained for the same parameter values as Fig. 6. Similar behavior is observed for an algebraic distribution of wave numbers.

zooming into other regions. When zooming into streaming regions, for example, what appears is either a better resolved streaming region or small eddies that are not resolved without appropriately zooming in. The fact that one can zoom into particular locations of a streaming region without seeing the fractal-eddy structure of the flow is not uncharacteristic of fractal structures. One of the most commonly cited ex-

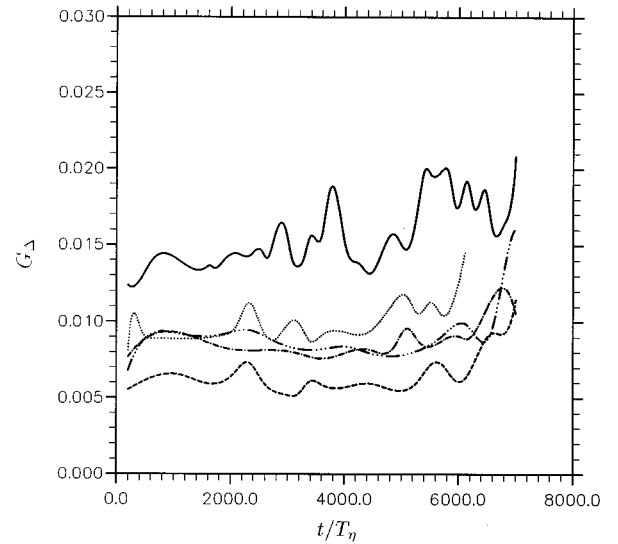


FIG. 15. Linear plot of G_{Δ} against t/T_{η} , where $T_{\eta} = \eta/\sqrt{E_0}$. This plot has been obtained for the same parameter values as Fig. 6, in particular $p=5/3$ and $\lambda=0.5$. The solid line corresponds to a geometric distribution of wave numbers and $N_k=79$. All the other lines correspond to an algebraic distribution, which $N_k=40$ (dashed), $N_k=79$ (dot-dashed), $N_k=125$ (triple-dot-dashed) and $N_k=158$ (dotted).

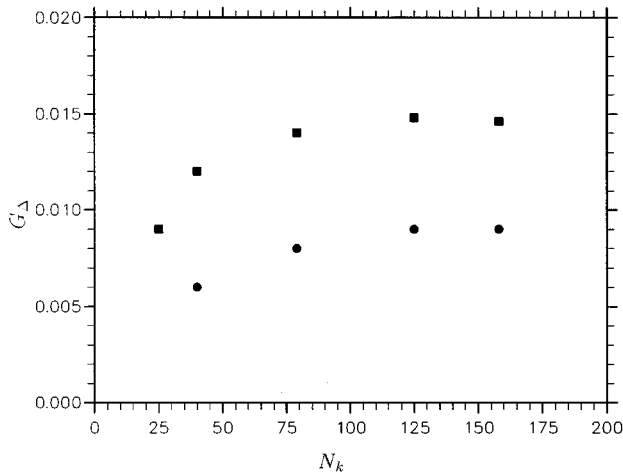


FIG. 16. Linear plot of G_Δ against the number N_k of wave modes. Parameter values are the same as for Fig. 15. Algebraic distribution of wave numbers (●), geometric distribution of wave numbers (■).

amples of a fractal is the triadic Cantor set and one cannot see its fractal structure if one zooms into the wrong empty regions between points of the set, and such empty regions exist at all scales. For $p \geq 3$ (not shown here for economy of space) however, such a fractal-eddy structure does not exist and no extra topological feature is uncovered by zooming into increasingly small scales inside eddies.

C. Richardson's constant G_Δ

Richardson's constant G_Δ is well defined when the power law (9) is well defined, and when $p=5/3$ the power law (9) is best defined for λ around 0.5 in which case G_Δ turns out to be $O(10^{-2})$.

In the derivation of the locality scaling (9) and (10) from the locality assumption (8) the constant G_Δ depends on the unsteadiness but is also a function of the dimensionless pa-

rameters p and N_k . The dependence of G_Δ on p and N_k throws some light onto the dependence of G_Δ on the topology of individual realizations of the flow. In Fig. 13 we plot the dependence of G_Δ on p for $\lambda=0.5$ and see that G_Δ decreases quite sharply from $p=1.2$ to $p=1.8$. As p increases the largest eddying regions in individual realizations of the turbulentlike flow grow in size relative to the fixed outer length scale L (see Vassilicos and Fung [19]). As demonstrated in Fig. 14, these larger eddying regions seem to occur at the expense of a smaller number of straining regions per unit area of the flow. In Fig. 14 we plot the straining-region density against the exponent p and show that this straining-region density decreases with increasing values of p . Following the arguments of Fung *et al.* [7], the value of G_Δ should therefore be smaller because the density of straining regions is smaller. Hence, the decreasing value of G_Δ with p is consistent with the idea [7] that particle pairs move together in eddying and streaming regions and separate violently in straining regions.

At a fixed Reynolds number $Re=(L/\eta)^{4/3}$, G_Δ is an increasing function of N_k , which does, however, appear to asymptote to a constant independent of N_k when N_k is larger than about 100 (see Figs. 15 and 16; for $N_k=500$ and all other parameters as for these figures, we obtain $G_\Delta=0.0082$ and $G_\Delta=0.015$, respectively, for the algebraic and geometric distributions of wave numbers, thus corroborating the asymptotic values in Fig. 16.) It may be unexpected to find that G_Δ can differ by as much as a factor of 2 for different distributions of wave numbers k_n (Figs. 15 and 16). We refer the reader to Sec. II C in Vassilicos and Fung [18] where it is explained how, for the same energy spectrum, subtle differences in wave-number distribution can dramatically change the topology of a field, and in particular the spatial distribution of maxima and minima of that field (Vassilicos and Fung [18] discuss the examples of Weierstrass, Riemann, and other such functions consisting of sums of sine waves). Such changes in topology may be expected to affect two-particle dispersion quantities such as G_Δ , but we leave

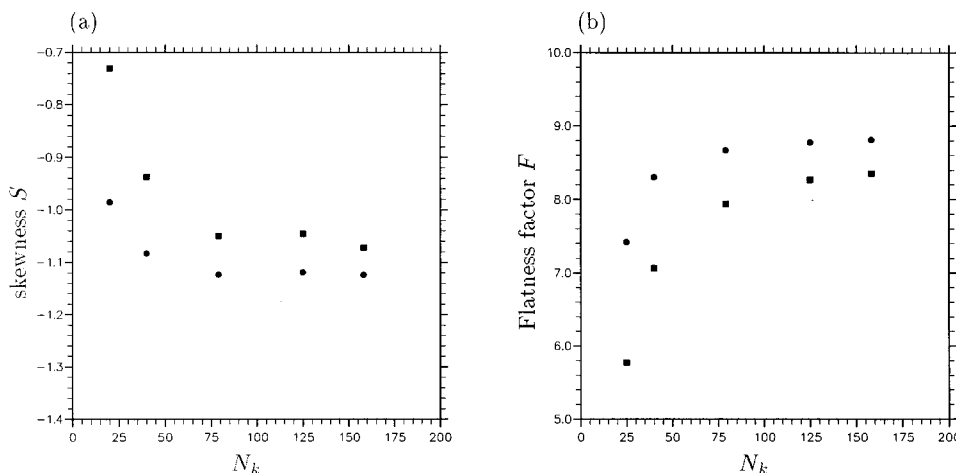


FIG. 17. Linear plots against the number N_k of wave modes of (a) the skewness S and (b) the flatness F of the Lagrangian distributions of second invariants II sampled along the particle trajectories. Parameter values are the same as for Figs. 15 and 16, in particular $p=5/3$ and $\lambda=0.5$. Algebraic distribution of wave numbers (●), geometric distribution of wave numbers (■).

for subsequent study this sensitive dependence of G_Δ on the details of the wave-number distribution. However, we do attempt to gain some understanding of the dependence of G_Δ on N_k .

We sample the values of the second invariant $II = (\partial u_i / \partial x_j)(\partial u_j / \partial x_i)$ along particle trajectories and calculate the skewness [Fig. 17(a)] and the flatness [Fig. 17(b)] of II from this Lagrangian sample. The average $\langle II \rangle$ over this Lagrangian sample is $\langle II \rangle = 0$, and therefore the skewness is $S = \langle II^3 \rangle / \langle II^2 \rangle^{3/2}$ and the flatness is $F = \langle II^4 \rangle / \langle II^2 \rangle^2$, where the angle brackets denote averages over the Lagrangian sample of second invariants II . In Fig. 17 we plot S and F against N_k and see that S decreases towards a constant value around -1.1 whereas F increases towards somewhere between 8.5 and 9. A negative value of the skewness of II that is smaller than -1.0 strongly suggests that during their flight particles visit eddying regions much more often than other regions [24,25]. However, a flatness of II that is much larger than 3 (the flatness of a Gaussian distribution) implies that extreme values of II , whether positive or negative, are more likely than for a normal (Gaussian) process. Hence, as N_k increases, more eddying and straining regions are visited by the particles [24,25], and even though the behavior of the skewness S indicates that particles are more often in eddying regions than in straining regions, the increase of G_Δ with N_k is consistent with the increase in the frequency of straining region visits that is reflected in the flatness of II . The fact that S decreases rather than increases with N_k is consistent with the low value of G_Δ , which remains $O(10^{-2})$ (when $p = 5/3$) for all values of N_k . A sharp increase of S with N_k would have resulted in much higher values of G_Δ because straining regions would have then been visited more often than eddying regions.

IV. SUMMARY OF CONCLUSIONS

The summary of our conclusions is as follows:

(i) The locality scaling $\overline{\Delta^2} = G_\Delta(E_0 L^{1-p})^{2/(3-p)} t^{4/(3-p)}$ is valid over the largest possible range provided that $p < 3$ and that the unsteadiness is neither too strong nor too weak, specifically $\lambda \approx 0.5$ or $U \approx 0.25\sqrt{E_0}$.

(ii) Individual realization of turbulentlike flows are topologically different above and below $p = 3$. When $p < 3$, 2D turbulentlike flows have a fractal-eddy structure that consists of cat's eyes within cat's eyes as schematically illustrated in

Fig. 12. When $p \geq 3$ no fractal-eddy structure exists, and eddying regions are simple without extra topological features appearing by zooming into increasingly small scales inside them.

(iii) When $p = 5/3$, $G_\Delta = O(10^{-2})$ as in Tatarski's measurements [6]. However, G_Δ can change by a factor of 2 simply by changing the distribution of modes in wave-number space. G_Δ is a decreasing function of p and an increasing function of the number of modes, N_k . The low value of G_Δ and the ways of these dependencies are consistent with the idea (proposed by Fung *et al.* [7]) that two-particle dispersion is effectively happening in bursts (see Fig. 1) when particle pairs meet straining regions. This idea is investigated quantitatively by measuring the skewness S and the flatness F of the second invariant II sampled along particle trajectories. The skewness S decreases to a constant value of -1.1 and the flatness F increases to a constant value between 8.5 and 9.0 with increasing N_k . Particles are therefore more often in eddying regions than in straining regions, but also more often in both eddying regions and straining regions for increasing values of N_k .

This paper is an attempt to articulate together the three central issues of this paper: the locality assumption, the fractal-eddy structure, and the straining regions' role in separating particle pairs in bursts. For 2D turbulentlike flows, we propose to sharpen the locality assumption that "in the inertial range, the dominant contribution to the turbulent diffusivity $(d/dt)\overline{\Delta^2}(t)$ comes from "eddies" of size $(\overline{\Delta^2})^{1/2}(t)$," where the word "eddies" has no clear topological meaning, by replacing it with: "in the inertial range, the dominant contribution to the turbulent diffusivity $(d/dt)\overline{\Delta^2}(t)$ comes from straining regions of size $(\overline{\Delta^2})^{1/2}(t)$; these straining regions are embedded in a fractal-eddy structure of cat's eyes within cat's eyes and therefore straining regions exist with a variety of length scales over the entire inertial range."

ACKNOWLEDGMENTS

The bulk of this work was carried out when J.C.H.F. was visiting the Department of Applied Mathematics and Theoretical Physics of the University of Cambridge as a Visiting Scholar of Wolfson College, Cambridge in 1995. Support from the Royal Society and from the Hong Kong Research Grant Council are gratefully acknowledged.

[1] P. A. Durbin, *J. Fluid Mech.* **100**, 279 (1980).
 [2] *Collected Papers of Lewis Fry Richardson*, edited by O. M. Ashford, H. Charnock, P. G. Drazin, J. C. R. Hunt, P. Smoker, and I. Sutherland (Cambridge University Press, Cambridge, 1993).
 [3] A. Obukhov, *Bull. Acad. Sci. U.S.S.R., Géog. & Géophys., Moscow* **5**, 453 (1941).
 [4] G. K. Batchelor, *Q. J. R. Meteorol. Soc.* **76**, 133 (1950).
 [5] G. K. Batchelor, *Proc. Cambridge Philos. Soc.* **48**, 345 (1952).

[6] V. I. Tatarski, *Izv. Vyssh. Uchebn. Zaved. Radiofiz.* **4**, 551 (1960).
 [7] J. C. H. Fung, J. C. R. Hunt, N. A. Malik, and R. J. Perkins, *J. Fluid Mech.* **236**, 281 (1992).
 [8] R. H. Kraichnan, *Phys. Fluids* **9**, 1937 (1966).
 [9] T. S. Lundgren, *J. Fluid Mech.* **111**, 27 (1981).
 [10] M. Larcheveque and M. Lesieur, *J. Mecanique* **20**, 113 (1981).
 [11] E. A. Novikov, *Sov. Phys. JETP* **17**, 1449 (1963).
 [12] S. Grossman and I. Procaccia, *Phys. Rev. A* **29**, 1358 (1984).

- [13] D. J. Thomson, *J. Fluid Mech.* **210**, 113 (1990).
- [14] M. S. Borgas and B. L. Sawford, *J. Fluid Mech.* **279**, 69 (1994).
- [15] K. Sabelfeld, *Monte Carlo Methods* (Springer-Verlag, Berlin, 1991).
- [16] F. W. Elliott and A. J. Majda, *Phys. Fluids* **8**, 1052 (1996).
- [17] H. van Dop, F. T. M. Nieuwstadt, and J. C. R. Hunt, *Phys. Fluids* **28**, 1639 (1985).
- [18] C. Turfus and J. C. R. Hunt, *Advances in Turbulence* (Springer-Verlag, Berlin, 1986).
- [19] J. C. Vassilicos and J. C. H. Fung, *Phys. Fluids* **7**, 1970 (1995).
- [20] P. Morel and M. Larcheveque, *J. Atmos. Sci.* **31**, 2189 (1974).
- [21] G. K. Batchelor, *The Theory of Homogeneous Turbulence* (Cambridge University Press, Cambridge, 1953).
- [22] W. H. Press, B. P. Flannery, S. A. Teukolsky, and W. T. Vetterling, *Numerical Recipes: The art of Scientific Computing* (Cambridge University Press, New York, 1986).
- [23] G. I. Taylor, *Proc. London Math. Soc. Ser 2*, **20**, 196 (1921).
- [24] A. A. Wray and J. C. R. Hunt, in *Proceedings of IUTAM Symposium on Topological Fluid Mechanics*, edited by H. K. Moffatt and A. Tsinober (Cambridge University Press, Cambridge, 1990).
- [25] J. C. H. Fung, J. C. R. Hunt, R. J. Perkins, A. A. Wray, and D. D. Stretch, in *Proceedings of the Third European Turbulence Conference, Stockholm, 1990*, edited by Johansson and Alfredsson (Springer-Verlag, Berlin, 1991).